

# Can We Find Neurons that Cause Unrealistic Images in Deep Generative Networks?

Hwanil Choi, Wonjoon Chang, Jaesik Choi\*

Graduate School of AI, KAIST, Seongnam, Republic of Korea

{hwanil.choi, one\_jj, jaesik.choi}@kaist.ac.kr

## Abstract

Even though image generation with Generative Adversarial Networks (GANs) has been showing remarkable ability to generate high-quality images, GANs do not always guarantee photorealistic images will be generated. Sometimes they generate images that have defective or unnatural objects, which are referred to as ‘artifacts’. Research to determine why the artifacts emerge and how they can be detected and removed has not been sufficiently carried out. To analyze this, we first hypothesize that rarely activated neurons and frequently activated neurons have different purposes and responsibilities for the progress of generating images. By analyzing the statistics and the roles for those neurons, we empirically show that rarely activated neurons are related to failed results of making diverse objects and lead to artifacts. In addition, we suggest a correction method, called ‘sequential ablation’, to repair the defective part of the generated images without complex computational cost and manual efforts.

## 1 Introduction

Generative Adversarial Networks (GANs) have been showing excellent performance for creating photo-realistic images, such as human faces, cars, and buildings. [Karras *et al.*, 2019; Brock *et al.*, 2019; Karras *et al.*, 2020; Chen and Yang, 2021; Esser *et al.*, 2021; Karras *et al.*, 2021]. Additionally, GANs can be used to synthesize a new realistic image from several real images. For example, a target human image can be transformed to obtain another’s face [Kim *et al.*, 2021]. These various uses of GANs have been utilized in many applications [Hung *et al.*, 2021; Chen and Yang, 2021; Liu *et al.*, 2021; Wang *et al.*, 2021].

Even though it is known that GANs have sufficient representative capacity to generate high-quality images, recent studies show that GANs still produce unrealistic images [Odena *et al.*, 2016; Bau *et al.*, 2018] or only generate limited types of samples. In this context, even PGGAN [Karras *et al.*, 2018] and StyleGAN [Karras *et al.*, 2020], which

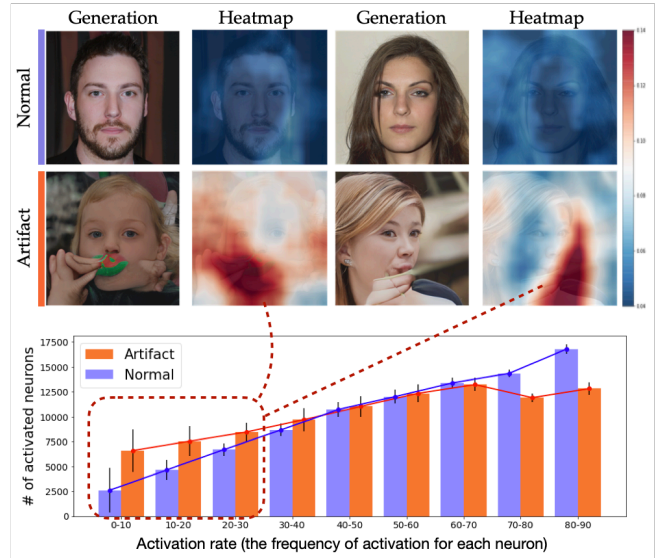


Figure 1: Heatmaps of rarely activated neurons for generated images. The first and second rows show the discrepancy between normal and artifact images respectively. The second and fourth columns describe the ratio of rarely activated neurons in featuremaps. In the red-colored area, where rarely activated neurons are activated a lot, there exist defective parts in the generated images. The bar plot shows that artifact images are highly related to rarely activated neurons compared to well-generated images.

are recognized as the high-performance models, may generate unrealistic images that include defective parts or unnatural objects, that is, artifacts. When artifacts are still emerging in image generation, the application of GANs will be limited. Recently, there have been some trials to identify the artifacts.

GAN-Dissection [Bau *et al.*, 2018] analyzes internal units in a pre-trained GAN to identify which units contribute to generating a specific object in a generated image. In this work, the authors found several units that are responsible for typical artifacts. One method to identify artifact is to find manually corresponding units creating artifacts. The other for automatic identification of artifacts units is using unit-specific FID scores. Then they turn off each identified unit, which means that activation values of all neurons in the selected unit are set to zero. Automatic Correction of Internal

\*Corresponding Author

Units in Generative Neural Networks [Tousi *et al.*, 2021] exploits an auxiliary classifier that is trained to distinguish artifacts from normal images. It requires handcrafted labels for fine-tuning this classifier. Grad-CAM [Selvaraju *et al.*, 2019], which shows areas that potentially contribute to the final result of classifier, is applied to identify the locations of defective parts. However, these studies lack analysis on the root of artifacts from the perspective of the generating process and they require manual sorting or additional training costs.

In this work, we focus on revealing what neurons makes images distorted, how artifacts can be detected, and what condition can make high quality natural images. In particular, we analyze PGGAN and StyleGAN2, which are the state-of-the-art model and have been widely adopted as the basic structures of generative models for high-quality resolution [Chen *et al.*, 2020; Kim *et al.*, 2021; Yao *et al.*, 2021]. We first analyze the frequency of activated neurons to reveal the behavior of the generating process. Figure 1 illustrates the relation between defective parts of generated images and rarely activated neurons, which we will define as ‘low frequency rate’. We will empirically verify that defective parts in the artifact images are corresponding to neurons with low frequency rate. From this analysis, we show that artifact can be censored without any additional cost. Furthermore, we propose an ablation method to remove defective parts with an unsupervised manner. This method doesn’t need any additional training procedure. This experiment supports our hypothesis with qualitative and quantitative results. The main contributions of our work are as follows:

- We analyze the frequency of activation in feature maps in order to reveal the properties of the generating procedure.
- We show experimentally that not only the artifacts are related to the rarely activated neurons, but also the artifacts are detected by this property.
- We provide qualitative and quantitative results to verify that artifacts are related to rarely activated neurons. Furthermore, our analysis can be applied to detect and remove artifacts of generated images.

## 2 Related work

### 2.1 Generative Adversarial Networks

GANs [Goodfellow *et al.*, 2014] have been leading a new paradigm of generative models. A GAN consists of a discriminator and a generator. The discriminator classifies between two images distributions: real images and fake images. The generator creates fake images to deceive the discriminator. The one of the improved version of conventional GAN structure is Progressive Growing GAN [Karras *et al.*, 2018]. This is trained sequentially by increasing the resolution and come to be one of the high-quality models. While recent models based on the GAN structure produce indistinguishable photo-realistic images, there have been few studies on the inner process of the GAN model.

### 2.2 Style-based GAN

StyleGAN [Karras *et al.*, 2019] was proposed as a novel generating mechanism for GAN to generate high quality and resolution images. This model has two parts: a mapping network and a style generator. The former transforms an input latent code  $z$  to a style code  $w$ . The latter generates an image with the trained constant tensor and the style vector  $w$ . Although StyleGAN affords good performance, the authors find blob artifacts in images. In order to address this, they suggested an advanced version, StyleGAN2 [Karras *et al.*, 2020]. Despite their efforts to remove specific artifacts such as blobs, the general artifacts remain unresolved. In addition, they propose a method improving image quality, called ‘truncation’. This makes the style vector located near the average style vector that is calculated on training time. However, the authors mentioned this truncation method hurts the diversity of output images.

### 2.3 Semantic Hierarchy Emerges in GAN

A recent study [Yang *et al.*, 2021] revealed the hierarchy mechanism of generative models. The authors noted that the generation process is the same as an artist drawing a picture by interpreting it from multiple abstraction levels. In the GAN models, the early layers create the layout of the output image. The middle layers create objects and attributes. Finally, the color scheme is rendered on the late layers. This implies that the artifacts are likely to occur in the early layers.

### 2.4 Detecting and removing Artifacts in Generative Models

In recent studies, GAN Dissection [Bau *et al.*, 2018] and Automatic Correction of Internal Units in Generative Neural Networks [Tousi *et al.*, 2021] have struggled to understand the inner mechanism of GANs. They suggest how the units occurring artifact are detected and fixing internal errors in the GAN so that the generator can provide realistic images without artifacts. GAN Dissection removes the internal units that are expected to cause defective elements. The latter trains an auxiliary neural network classifier. For the case of an artifact image, the auxiliary classifier is used to search a region that is considered to be strange by applying Grad-CAM [Selvaraju *et al.*, 2019].

## 3 Analysis for the Frequency Rate

In this section, we attempt to shed light on the causes of the diversity of generated images by observing the frequency of activation of internal neurons in GAN, which may lead to the generation of artifacts. We first explain notations for GAN structure to define frequency rate of neurons. According to the frequency rate, we verify that rarely activated neurons are highly related to unusual features and defective parts in generated images by analyzing the effects of those neurons. Furthermore, we suggest an efficient detection and ablation technique based on our analysis.

### 3.1 The Frequency Rate of Neurons

**Hypothesis** In featuremaps of generated images, some neurons are rarely activated whereas other neurons are frequently

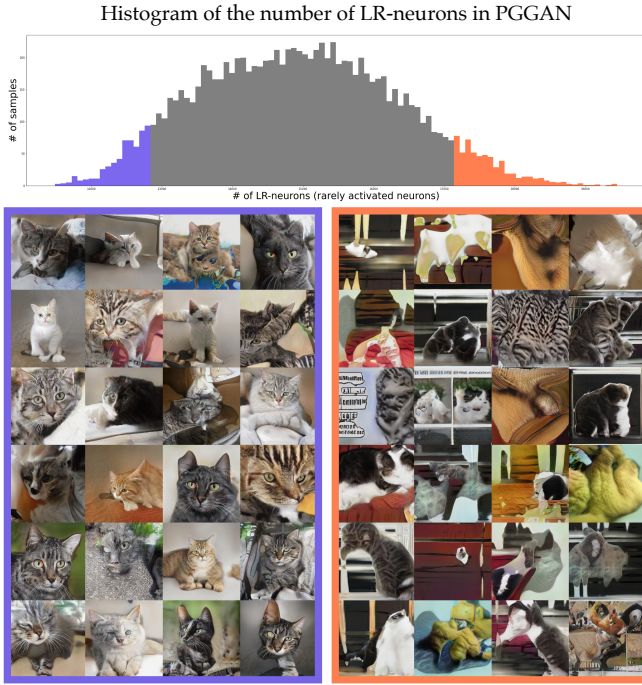


Figure 2: Generated images according to the number of rarely activated neurons in PGGAN. (Left) The samples in the blue box, of which featuremaps are composed mostly of frequently activated neurons, have general cat images. (Right) The samples in the red box have diverse components, but most of them fail to construct realistic cat images.

activated. In other words, neurons have different activation frequency, which will be precisely defined as the ‘frequency rate’ in Definition 2. We observe that featuremaps of normal images among generated results are composed mostly of frequently activated neurons. For instance, rare cases in Figure 3 have neurons with low frequency rate a lot in their featuremaps unlike general cases. In this spirit, we hypothesize that rarely activated neurons are used to create diverse components including failures and frequently activated neurons are used to construct general components that are necessary for realistic images.

Figure 2 provides empirical evidence of our hypothesis. The histogram shows the number of generated images according to the number of activated neurons that are rarely activated during the generating procedure. The images in the red box, of which featuremaps have rarely activated neurons a lot, have diverse components like images with phrases. Most of them, however, fail to construct realistic images, while the images in the blue box show general cat images. It is reasonable to suspect that rarely activated neurons would be highly related to artifact images generated from GANs.

For convenience, we introduce some notations for GAN structure and define the activation rate to measure the frequency of activations. GAN consists of two parts, a generator  $G : \mathcal{Z} \rightarrow \mathcal{I}$  generates an output image where  $\mathcal{Z}$  is a latent vector space and  $\mathcal{I}$  is the space of output images. Since we analyze the process

of image generation and internal neurons, we determine the generator  $G$  as our main target. A function from the 0 th layer to the  $i$  th layer of the generator is denoted by  $G^{i:i}$ . The output of the  $i$  th layer is denoted by  $f^i(\mathbf{z}) = G^{(i-1):i}(f^{(i-1)}(\mathbf{z}))$ , where  $f^0(\mathbf{z}) = G^0(\mathbf{z})$ .

**Definition 1 (Activated Neuron).** *Given a generator  $G$  and its featuremap  $f^i(\mathbf{z})$  for the  $i$  th layer, the activation value of the  $n$  th neuron is defined by  $f_n^i(\mathbf{z})$ . We called it ‘activated’ if  $f_n^i(\mathbf{z}) > 0$ . In particular, the set of the activated neurons in the  $i$  th layer is defined by  $[f^i]^+$ .*

**Definition 2 (Neurons with Activation Rate  $R$ ).** *Given a featuremap  $f^i$ ,  $R_n^i$  is the probability that a neuron  $f_n^i(\cdot)$  is activated.  $\mathcal{R}_{n,R}^i$  is the set of neurons with activation rate  $R$  such that  $R_n^i = R$ .*

For each neuron, activation rate  $R$  denotes how frequently the neuron is indeed activated. Since the true probability for each neuron cannot be computed exactly, we samples 30K latent codes to estimate the relative frequency  $R_n^i$ :

$$R_n^i = \frac{1}{N} \sum_{k=1}^N I(f_n^i(\mathbf{z}_k) > 0) \quad (1)$$

where  $I$  is the indicator function and  $N = 30K$ . We analyze the effect of neurons with a low frequency rate and that of neurons with a high frequency rate. Then, with the constant rate  $R$ , we denote the set of neurons which have  $R_n^i > R$  by  $\mathcal{F}_{\cdot,R}^i$  and denote the set of neurons that have  $R_n^i \leq R$  by  $\mathcal{F}_{\cdot,R}^i$ . When there is no confusion in the context, we simply call  $\mathcal{F}_{\cdot,R}^i$  ‘HR-neurons’ (high rate neurons) and call  $\mathcal{F}_{\cdot,R}^i$  ‘LR-neurons’ (low rate neurons).

### 3.2 Relationship between Frequency Rate and Generations

To observe the effects of neurons according to their frequency rates, we first introduce an ablation method, namely ‘Sequential Ablation’, in Algorithm 1. Given a latent code  $\mathbf{z} \in \mathcal{Z}$ ,

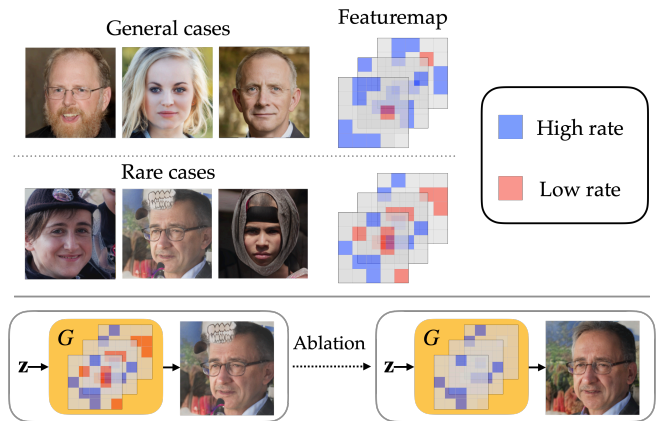


Figure 3: (Top) Comparison of feature maps between general samples and rare samples and (Bottom) our proposed ablation process. The red color denotes rarely activated neurons and the blue color denotes frequently activated neurons.

---

**Algorithm 1** Sequential Ablation

---

**Input:** Generator  $G$ , A latent code  $\mathbf{z} \in \mathcal{Z}$ 
**Parameter:** All Layer index list  $\mathbf{L}$ , Layer index list  $\mathbf{M}$  for ablation, Activation rate  $R$ 
**Output:** Corrected Image  $I_{corr}$ 

```

1: Let  $I \leftarrow \mathbf{z}$ .
2: for  $i$  in  $\mathbf{L}$  do
3:    $f^i \leftarrow G^{(i-1):i}(I)$ 
4:   if  $i$  in  $\mathbf{M}$  then
5:      $[f^i]_{:,R} \leftarrow 0$ 
6:   else
7:     do not anything
8:   end if
9:    $I \leftarrow f^i$ 
10: end for
11:  $I_{corr} \leftarrow I$ 
12: return  $I_{corr}$ 

```

---

it iteratively computes its featuremap while turning off activated LR-neurons for each layer. That is, it makes values of activated LR-neurons as zeros. The target layers to remove LR-neurons are limited to indices in  $\mathbf{M}$ , since neurons on different layers may have different effects on generated images. It has been studied that each layer in GANs plays a different role in generating process in a hierarchical manner [Yang *et al.*, 2021]. The authors noted that the early and middle layers determine the spatial layout and the objects, and the last layers render the attributes and color scheme. Therefore, we set  $\mathbf{M}$  to include the early or middle layers of the generator, since our work focuses on analyzing the root of unrealistic objects or defective parts.

### Analysis for Layer

For one randomly selected artifact image generated from StyleGAN2, the first row in Figure 4 shows how LR-neurons are distributed in its featuremap for each layer. The generated image has a strange object on its chin and a grid-like background. The red part of heatmaps indicates the high proportion of LR-neurons. Heatmaps on layers 5 and 7 have a large number of LR-neurons at the chin. The second row shows heatmaps and the third row shows generated images, when applying sequential ablation until the previous layers. That is, the heatmap of layer 5 in the second row denotes the heatmap when applying sequential ablation at layers 0, 1, 3. Through sequential ablation, LR-neurons at the defective parts of the chin are removed and the generated image is also repaired successfully. Therefore, we can identify that LR-neurons in the early layers are highly related to make defective parts. However, when we apply sequential ablation for the higher layers, most of the background part disappear and the hairstyle become different. It implies that LR-neurons in layers 5 and 7 contributes to constructing detail features or background. From this result, we conclude that applying sequential ablation until layer 3 is an appropriate choice to repair generated images without hindering the diversity of gen-

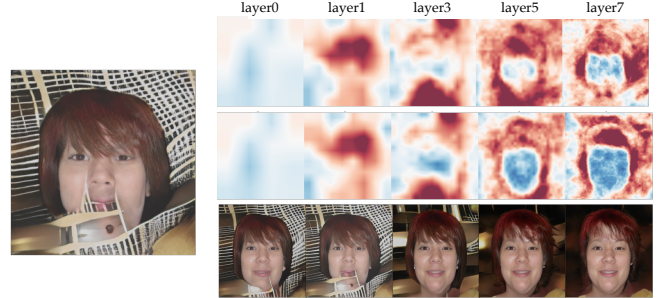


Figure 4: Heatmaps of neurons with low frequency rate and their effects on generations. The left most column is generated artifact image. The first row shows the masks of activations corresponding to  $[f^i_{:,0.3}]^+$ . The second row shows the masks of activations that are applied sequential ablation upto a given layer. The third row describes the generated images after sequential ablation.

erations. In Section 4.2, artifact correction results in Table 1 will support our determination quantitatively.

### Analysis for Rate

In this section, we provide qualitative analysis to verify our hypothesis and reveal the roles of neurons according to the frequency rate. Figure 5 shows the generation results of StyleGAN2 with applying sequential ablation in layers 0, 1, 3 with different rates on FFHQ, LSUN-Cat, and LSUN-Church. In this analysis, we remove not only LR-neurons but also HR-neurons to identify the effects of HR-neurons even though sequential ablation originally denotes ablating LR-neurons. For each generated image, the first row shows results from ablating HR-neurons with a given  $R$  and the second row shows results from ablating LR-neurons.

When ablating HR-neurons, the basic structures of the objects, such as shapes of faces, totally collapse. Uncommon characteristic, such as the blue artifact in the first cat image and the human-like artifact in the third cat image, still remain after ablating HR-neurons. Even though the remaining neurons, which are rarely activated, may be necessary parts to generate images with diverse properties, they easily hinder visual fidelity.

Artifacts in the generated images are removed when we ablates LR-neurons. Distorted hands in the generated human images successfully disappear with  $R = 0.3$  or  $0.5$ . The watermark in the second cat image and the second church image are eliminated, and their shapes become more natural. However, ablating  $[f^i_{:,0.5}]^+$  may remove too much information so that generated images have only fundamental components and lose own properties. In this case,  $R = 0.3$  is a valid choice for sequential ablation to remove defective parts while maintaining the details.

### 3.3 Ablating Neurons to Repair Artifacts

From our previous analysis, we observe that LR-neurons in the early layers are highly related to generate defective parts in the results. In this spirit, we propose an efficient ablation method to avoid generating artifact images. It follows ‘Sequential Ablation’ method, which is described in Algorithm 1, and we set the early layers as a list of target layers

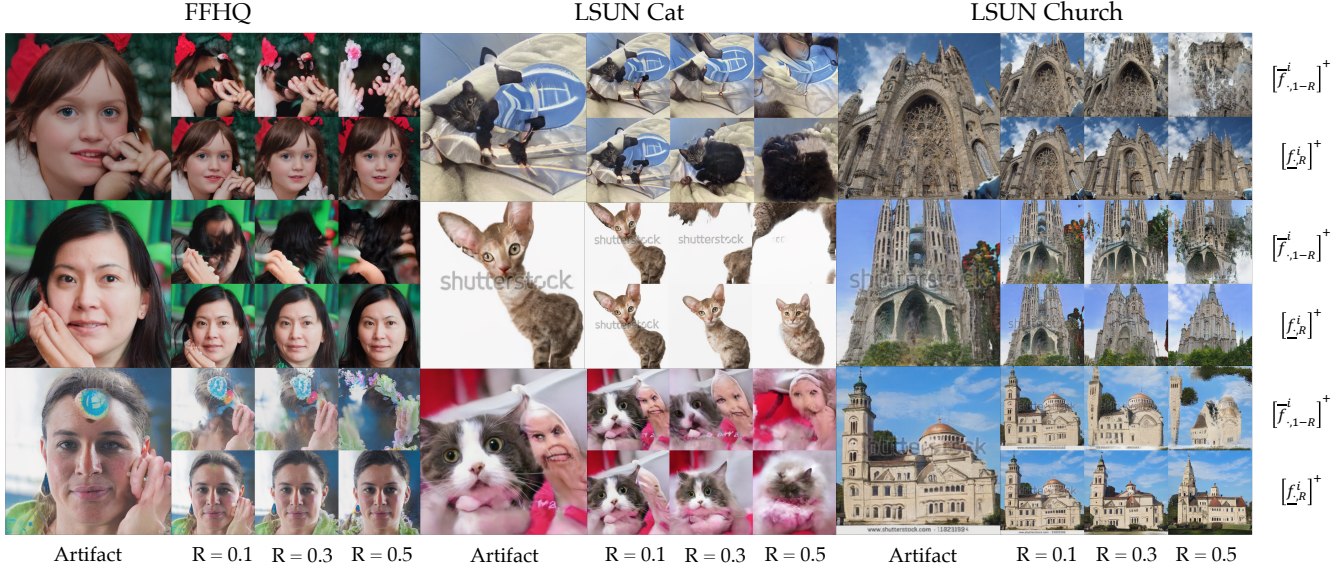


Figure 5: Generated images from StyleGAN2 with ablating HR-neurons or LR-neurons. For each sample, the first row shows the results of ablating HR-neurons, and the second row shows the results of ablating LR-neurons.

Layers	None	0	1	3	0,1	0,1,3	0,1,3,5
$[f^i_{0,0.7}]^+$	240.8	241.2	259.0	233.3	277.7	342.5	
	<b>36.3</b>	<b>31.6</b>	33.4	<b>30.9</b>	38.5	56.7	
	48.9	44.9	37.0	<b>31.9</b>	35.6	<b>29.6</b>	39.2
		48.7	46.9	41.5	46.8	40.3	<b>38.3</b>
		74.1	124.1	118.6	147.2	155.1	163.0
		43.5	44.5	55.4	52.4	178.0	226.7

Table 1: FID scores for repaired images with various target layer indices and rate  $R$  in StyleGAN2 with the FFHQ dataset.

$M$  with  $R = 0.3$ . Experiment 4.2 will show that this setting is valid.

Figure 3 describes the overall correction process. Otherwise, we denote applying ablation only for a single layer by ‘Single Ablation’. In Table 1, we use single ablation to compare the performance. Note that our ablation method does not require complex computations or manual analysis in the repair process. We can easily repair the image by setting activated LR-neurons as zero.

## 4 Experiment

In this section, we carry out following qualitative and quantitative experiments to evaluate our approach. The main results show the relationship between LR-neurons and low visual fidelity (or artifacts). We use the codes reproduced by PyTorch from genforce github [Shen *et al.*, 2020] that provides the official pre-trained weights<sup>1</sup>; PGGANs trained on CelebA-HQ, LSUN-Cat, and LSUN-Church and StyleGAN2s trained on FFHQ, LSUN-Cat, and LSUN-Church.

<sup>1</sup><https://github.com/genforce/genforce>

### 4.1 Qualitative Results

50K latent codes are randomly sampled to generate images without truncation method. The number of the total activated LR-neurons ( $R = 0.3$ ) in the early layers is counted in each generation, i.e., the sum of  $|\underline{f}^i_{0,0.3}]^+|$ . The target early layers are set to  $i = 1, 3, 5$  for PGGAN and  $i = 0, 1, 3$  for StyleGAN2. Dimensions of each layer’s output correspond to  $\mathbb{R}^{512 \times 4 \times 4}$ ,  $\mathbb{R}^{512 \times 8 \times 8}$ ,  $\mathbb{R}^{512 \times 16 \times 16}$ , respectively.

### Low fidelity detection in image generations

To detect images with low visual fidelity images, we sort the number of activated LR-neurons with decreasing order. Then we select Top 2K images and Bottom 2K images, corresponding to the sorted order. Figure 2 shows the histogram of the number of activated LR-neurons. The blue region means they have a few activated LR-neurons and the red region indicates that the generated images have a number of activated LR-neurons. Consistent with our hypothesis, the generated images in the red region, they have more defective or distorted parts than the images in the blue region. The images in the blue box have the high visual fidelity, but lack diversity, whereas the images in the red box seem to have more uncommon properties. We provide abundant results of detection tasks in Appendix B-G.

### Sequential Ablation

Figure 5 shows sequential ablation results of StyleGAN2 in FFHQ, LSUN-Cat, and LSUN-Church. The ablation method is conducted on layer 0, 1, and 3 with various rate  $R$  as described in Section 3.2. It supports that the LR-neurons induce the artifacts. Furthermore, as introduced in Section 3.3, we conduct sequential ablation to correct artifacts generated from StyleGAN2 and PGGAN. In Figure 3, we identify that our approach can repair the artifacts in various cases. In the

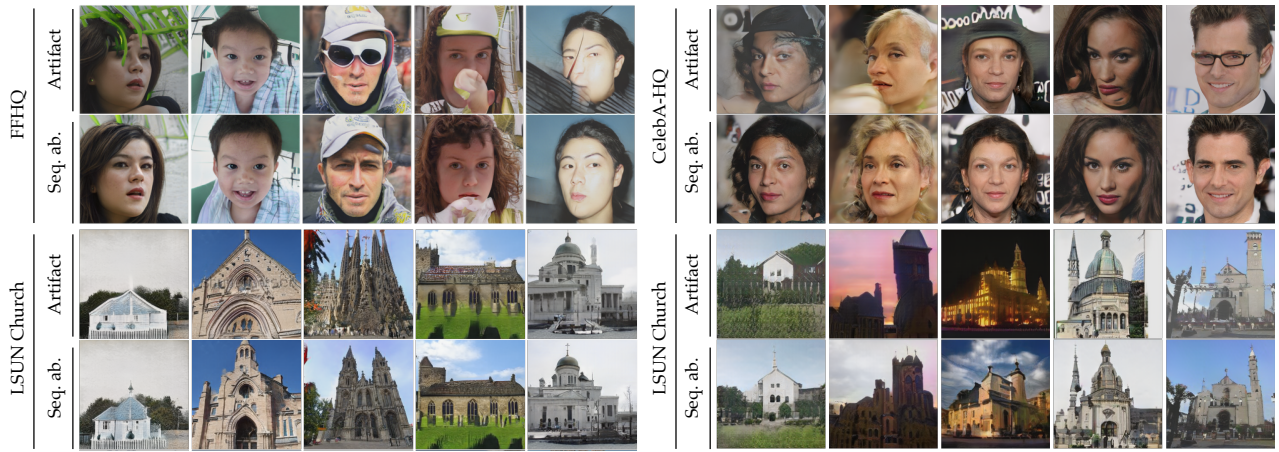


Figure 6: Sequential Ablation results for correcting artifacts in StyleGAN2s and PGGANs

	Datasets	Bottom 2K			Top 2K		
		Precision (fidelity)	Recall (diversity)	Realism Score	Precision (fidelity)	Recall (diversity)	Realism Score
PGGAN	CelebA-HQ	<b>0.9245</b>	0.1056	<b>1.0911±0.0712</b>	0.4565	<b>0.3194</b>	0.9942±0.0663
	LSUN-Cat	<b>0.8450</b>	0.0893	<b>1.0680±0.0686</b>	0.4745	<b>0.1089</b>	1.0011±0.0571
	LSUN-Church	<b>0.8985</b>	0.1907	<b>1.0754±0.0627</b>	0.4165	<b>0.3628</b>	0.9902±0.0697
StyleGAN2	FFHQ	<b>0.9085</b>	0.2153	<b>1.1112±0.0913</b>	0.762	<b>0.4763</b>	1.0370±0.0725
	LSUN-Cat	<b>0.9195</b>	0.1404	<b>1.0875±0.0704</b>	0.6385	<b>0.4025</b>	1.0206±0.0579
	LSUN-Church	<b>0.8315</b>	0.2226	<b>1.0631±0.0640</b>	0.4935	<b>0.3646</b>	1.0016±0.0729

Table 2: Precision, Recall, and Realism Score of Top/Bottom images with a lot/few of LR-neurons.

case of StyleGAN2, a long crack on the face of the fifth human image is eliminated successfully. The buildings are not constructed completely and mixed with their backgrounds in the artifact church images generated from PGGAN. After sequential ablation, the buildings are repaired normally. In addition, we provide more results in Appendix H (it includes the results of StyleGAN3 [Karras *et al.*, 2021] with FFHQ).

## 4.2 Quantitative Results

### Correction study

We evaluate our ablation method with various combinations of target layers and rate  $R$  in the FFHQ dataset with FID score [Heusel *et al.*, 2017]. Table 1 shows FID scores computed with 10K real images and 1.3K artifacts images. ‘None’ denotes that the case when we do not apply our ablation method and ‘Random’ denotes that we ablate 30% of activated neurons that are randomly selected. Note that we remove activated HR-neurons to identify the effects of HR-neurons on generations in the case of the 5th row.

As a result, the ablation result when turning off  $[f_{\cdot,0.3}^i]^+$  with  $i = 0, 1, 3$  has the best FID score. Compared to the case  $[f_{\cdot,0.3}^i]^+$ , the case  $[f_{\cdot,0.7}^i]^+$  has very high FID scores, since HR-neurons play significant roles to generate essential parts of images. We use the best setting ( $[f_{\cdot,R}^i]^+$  with  $R = 0.3, i = 0, 1, 3$ ) to conduct our qualitative experiments.

### Diversity and Fidelity

We quantify our detection method with the precision (fidelity), recall (diversity), and Realism Score [Kynkänniemi *et al.*, 2019] with 10K real images, Top 2K and Bottom 2K samples for each dataset, and the number of neighborhood  $k = 3$ . Table 2 shows that Bottom 2K samples that have the small number of LR-neurons cause high score in fidelity and realism score, but low score in recall. However, Top 2K samples that have the large number of LR-neurons shows that fidelity and realism score is lower than bottom samples, but diversity is higher in all cases. This results come to be the evidence of our hypothesis that too much diversity leads to artifacts. In addition, it may imply a trade-off between fidelity and diversity in the generation procedure.

## 5 Conclusion

In this paper, we suggest a hypothesis that rarely activated neurons are highly related to generating artifacts, which are indeed failures to create diversity. Our ablation study not only supports that low rate neurons in the early layers induce defective parts but also shows that frequently activated neurons may affect essential parts. As a result, our approach can detect artifact images and correct defective parts by sequential ablation without any supervision. The remaining problem is to overcome a trade-off between diversity and fidelity by breaking the connection of diversity and artifacts.

## References

[Bau *et al.*, 2018] David Bau, Jun-Yan Zhu, Hendrik Strobelt, Bolei Zhou, Joshua B Tenenbaum, William T Freeman, and Antonio Torralba. Gan dissection: Visualizing and understanding generative adversarial networks. *arXiv preprint arXiv:1811.10597*, 2018.

[Brock *et al.*, 2019] Andrew Brock, Jeff Donahue, and Karen Simonyan. Large scale GAN training for high fidelity natural image synthesis. In *International Conference on Learning Representations*, 2019.

[Chen and Yang, 2021] Zehao Chen and Hua Yang. Attentive semantic exploring for manipulated face detection. *ICASSP 2021 - 2021 IEEE International Conference on Acoustics, Speech and Signal Processing (ICASSP)*, Jun 2021.

[Chen *et al.*, 2020] Anpei Chen, Ruiyang Liu, Ling Xie, Zhang Chen, Hao Su, and Jingyi Yu. Sofgan: A portrait image generator with dynamic styling. *arXiv preprint arXiv:2007.03780*, 2020.

[Esser *et al.*, 2021] Patrick Esser, Robin Rombach, and Björn Ommer. Taming transformers for high-resolution image synthesis, 2021.

[Goodfellow *et al.*, 2014] Ian Goodfellow, Jean Pouget-Abadie, Mehdi Mirza, Bing Xu, David Warde-Farley, Sherjil Ozair, Aaron Courville, and Yoshua Bengio. Generative adversarial nets. *Advances in neural information processing systems*, 27, 2014.

[Heusel *et al.*, 2017] Martin Heusel, Hubert Ramsauer, Thomas Unterthiner, Bernhard Nessler, and Sepp Hochreiter. Gans trained by a two time-scale update rule converge to a local nash equilibrium. *Advances in neural information processing systems*, 30, 2017.

[Hung *et al.*, 2021] Tun-Min Hung, Bo-Yu Chen, Yen-Tung Yeh, and Yi-Hsuan Yang. A benchmarking initiative for audio-domain music generation using the freesound loop dataset, 2021.

[Karras *et al.*, 2018] Tero Karras, Timo Aila, Samuli Laine, and Jaakko Lehtinen. Progressive growing of gans for improved quality, stability, and variation. In *International Conference on Learning Representations*, 2018.

[Karras *et al.*, 2019] Tero Karras, Samuli Laine, and Timo Aila. A style-based generator architecture for generative adversarial networks. In *Proceedings of the IEEE/CVF Conference on Computer Vision and Pattern Recognition*, pages 4401–4410, 2019.

[Karras *et al.*, 2020] Tero Karras, Samuli Laine, Miika Aittala, Janne Hellsten, Jaakko Lehtinen, and Timo Aila. Analyzing and improving the image quality of stylegan. In *Proceedings of the IEEE/CVF Conference on Computer Vision and Pattern Recognition*, pages 8110–8119, 2020.

[Karras *et al.*, 2021] Tero Karras, Miika Aittala, Samuli Laine, Erik Härkönen, Janne Hellsten, Jaakko Lehtinen, and Timo Aila. Alias-free generative adversarial networks. *Advances in Neural Information Processing Systems*, 34, 2021.

[Kim *et al.*, 2021] Hyunsu Kim, Yunjey Choi, Junho Kim, Sungjoo Yoo, and Youngjung Uh. Exploiting spatial dimensions of latent in gan for real-time image editing, 2021.

[Kynkänniemi *et al.*, 2019] Tuomas Kynkänniemi, Tero Karras, Samuli Laine, Jaakko Lehtinen, and Timo Aila. Improved precision and recall metric for assessing generative models. *arXiv preprint arXiv:1904.06991*, 2019.

[Liu *et al.*, 2021] Mingcong Liu, Qiang Li, Zekui Qin, Guoxin Zhang, Pengfei Wan, and Wen Zheng. Blendgan: Implicitly gan blending for arbitrary stylized face generation, 2021.

[Odena *et al.*, 2016] Augustus Odena, Vincent Dumoulin, and Chris Olah. Deconvolution and checkerboard artifacts. *Distill*, 2016.

[Selvaraju *et al.*, 2019] Ramprasaath R. Selvaraju, Michael Cogswell, Abhishek Das, Ramakrishna Vedantam, Devi Parikh, and Dhruv Batra. Grad-cam: Visual explanations from deep networks via gradient-based localization. *International Journal of Computer Vision*, 128(2):336–359, Oct 2019.

[Shen *et al.*, 2020] Yujun Shen, Yinghao Xu, Ceyuan Yang, Jiapeng Zhu, and Bolei Zhou. Genforce. <https://github.com/genforce/genforce>, 2020.

[Tousi *et al.*, 2021] Ali Tousi, Haedong Jeong, Jiyeon Han, Hwanil Choi, and Jaesik Choi. Automatic correction of internal units in generative neural networks. In *Proceedings of the IEEE/CVF Conference on Computer Vision and Pattern Recognition*, pages 7932–7940, 2021.

[Wang *et al.*, 2021] Tuanfeng Y. Wang, Duygu Ceylan, Krishna Kumar Singh, and Niloy J. Mitra. Dance in the wild: Monocular human animation with neural dynamic appearance synthesis, 2021.

[Yang *et al.*, 2021] Ceyuan Yang, Yujun Shen, and Bolei Zhou. Semantic hierarchy emerges in deep generative representations for scene synthesis. *International Journal of Computer Vision*, 129(5):1451–1466, 2021.

[Yao *et al.*, 2021] Xu Yao, Alasdair Newson, Yann Gousseau, and Pierre Hellier. A latent transformer for disentangled face editing in images and videos, 2021.